NIH Public Access
Author Manuscript
Chemphyschem. Author manuscript; available in PMC 2013 October 22.

Published in final edited form as:
Chemphyschem. 2012 October 22; 13(15): 3481–3491. doi:10.1002/cphc.201200405.

Two-Photon Absorption and Time-Resolved Stimulated Emission Depletion Spectroscopy of a New Fluorenyl Derivative

Prof. Kevin D. Belfield[a],[b], **Mykhailo V. Bondar**[c], **Alma R. Morales**[a], **Ms. Xiling Yue**[a], **Dr. Gheorghe Luchita**[a], **Olga V. Przhonska**[c], and **Olexy D. Kachkovsky**[d]

Kevin D. Belfield: belfield@mail.ucf.edu; Mykhailo V. Bondar: mbondar@mail.ucf.edu

[a]Department of Chemistry University of Central Florida P.O. Box 162366, Orlando, FL 32816-2366, USA)

[b]CREOL, The College of Optics and Photonics University of Central Florida P.O. Box 162366, Orlando, FL 32816-2366, USA

[c]Institute of Physics National Academy of Sciences of Ukraine Prospect Nauki, 46, Kiev-28, 03028, Ukraine

[d]Insitute of Organic Chemistry, Murmanskaya Street, 5, Kiev, 03094, Ukraine

Abstract

The synthesis, comprehensive linear photophysical characterization, two-photon absorption (2PA), steady-state and time-resolved stimulated emission depletion properties of a new fluorene derivative, (E)-1-(2-(di-p-tolylamino)-9,9-diethyl-9H-fluoren-7-yl)-3-(thiophen-2-yl)prop-2-en-1-one (**1**), are reported. The primary linear spectral properties, including excitation anisotropy, fluorescence lifetimes, and photostability, were investigated in a number of aprotic solvents at room temperature. The degenerate 2PA spectra of **1** were obtained with an open aperture Z-scan and two-photon induced fluorescence methods, using a 1-kHz femtosecond laser system, and maximum 2PA cross-sections of ~400–600 GM were obtained. The nature of the electronic absorption processes in **1** was investigated by DFT-based quantum chemical methods implemented in the Gaussian 09 program. The one- and two-photon stimulated emission spectra of **1** were measured over a broad spectral range using a femtosecond pump probe–based fluorescence quenching technique, while a new methodology for time-resolved fluorescence emission spectroscopy is proposed. An effective application of **1** in fluorescence bioimaging was demonstrated via one- and two-photon fluorescence microscopy images of HCT 116 cells containing the dye encapsulated micelles.

Keywords

fluorene derivatives; two-photon absorption; two-photon stimulated emission depletion; time-resolved fluorescence spectroscopy; bioimaging

Introduction

The development of new organic molecules with efficient two-photon absorption (2PA) and stimulated emission depletion (STED) properties is a subject of enhanced scientific and technological interest for the manifold promising areas of nonlinear optical applications,

Correspondence to: Kevin D. Belfield, belfield@mail.ucf.edu.

Supporting information for this article is available on the WWW under http://www.chemeurj.org/ or from the author.

$watermark-text
$watermark-text
$watermark-text

$watermark-text

$watermark-text

$watermark-text

such as 3D optical data storage and microfibrication,[1–4] two-photon–induced fluorescence microscopy (2PFM),[5, 6] two-photon optical power limiting,[7, 8] high-resolution molecular spectroscopy,[9] light amplification of stimulated emission,[10, 11] etc. Investigations of the electronic structure of organic molecules and the nature of their spontaneous and stimulated intramolecular vibronic transitions have allowed for the designing of efficient 2PA compounds with high fluorescence quantum yields and large STED cross-sections in the region of interest.[12–14] The strategy for the development of effective 2PA molecules and the corresponding experimental methods for 2PA cross-section determination are well established and widely used,[15–17] in contrast to STED spectroscopic techniques, which can be utilized in nonlinear-optical measurements.[18, 19] It is worth noting that stimulated emission processes in organic molecules have great potential for a number of the practical applications mentioned above and need to be investigated further. One of the promising methods among these investigations is a fluorescence-quenching methodology described previously by Lakowicz.[20, 21] This method is based on the quenching of fluorescence emission which can occur within a single excitation pulse, or can be accomplished by a separate time-delayed laser pulse with corresponding wavelength. This technique allows investigations of ultrafast processes occurring in the excited states of fluorophores,[22, 23] as well as the most accurate determination of corresponding one- and two-photon stimulated emission cross-sections using high intensity pico- and femtosecond laser pulses.[14, 24] Based on these data, one- and two-photon STED spectra can be evaluated for further development in some practical areas, such as high-resolution multiphoton fluorescence microscopy,[25, 26] upconverting lasing,[27, 28] superfluorescent labels for bioimaging,[29, 30] etc. Among the tremendous number of organic compounds with efficient nonlinear-optical properties, fluorene derivatives are promising organic structures with high potential for most of the known laser-based spectroscopic applications.[16, 31, 32]

In this paper, the STED properties of a new fluorene derivative, (E)-1-(2-(dip-tolylamino)-9,9-diethyl-9H-fluoren-7-yl)-3-(thiophen-2-yl)prop-2-en-1-one (**1**), were investigated by a fluorescence-quenching femtosecond technique along with the comprehensive linear photophysical, photochemical, and 2PA characterizations of **1** in a broad variety of organic solvents at room temperature. Values of 2PA and stimulated-emission cross-sections of **1** were obtained in a broad spectral range with a 1-kHz tunable femtosecond laser system by open aperture Z-scan,[33] two-photon induced fluorescence (2PF),[34] and pump-probe fluorescence-quenching methods,[14] respectively. A time-resolved fluorescence spectrum method, based on STED pump-probe methodology, was proposed for the first time, and the values of the fast solvate relaxation constants for 1 in low viscosity media were evaluated. The nature of the electronic structure of 1 was also investigated using quantum-chemical calculations with DFT-based methods implemented in the Gaussian 09 program package.[35] High-fluorescence quantum yields, efficient 2PA and STED cross-sections, and good photochemical stability reveal the high potential of 1 for application in a number of important nonlinear-optical areas of use, including high-resolution STED microscopy.[25, 26] A high potential of 1 for application in bioimaging was shown via one- and two-photon fluorescence microscopy of epithelial colorectal carcinoma HCT 116 cells encapsulated in Pluronic® F-127 micelles.

Results and Discussion

Linear spectral and photochemical properties of 1

The linear absorption and fluorescence spectra of **1** in hexane (HEX), toluene (TOL), chloroform ($CHCl_3$), tetrahydrofuran (THF), and acetonitrile (ACN), along with the main photophysical and photochemical parameters, are presented in Figure 1 and in Table 1, respectively. The steady-state absorption spectra exhibited a weak dependence on the solvent properties, and a structureless shape was observed in all of the investigated aprotic

$watermark-text

$watermark-text

$watermark-text

solvents, except for nonpolar HEX. Well-defined vibronic absorption peaks were observed in the main long-wavelength absorption band of **1** (360 – 480 nm) in HEX solutions (Figure 1, curve 1), with spacings associated with C-C vibrations (~ 1080 cm^{-1}). The fluorescence spectra of **1** were independent of the excitation wavelength, λ_{ex} in the whole absorption range and exhibited a strong solvatochromic behavior with a maximum Stokes shift greater than ~180 nm in $CHCl_3$ (curve 4′). The values of fluorescence quantum yields, Φ, were sufficiently high (0.64 – 1.0) in all of the investigated solvents (except for polar ACN, see Table 1) and independent of λ_{ex} in the spectral range 280 – 480 nm. These results were consistent with nice overlapping of the absorption and corrected excitation spectra of **1** in a broad spectral range. This finding implies a strict correspondence to Kasha's rule,[36] which states that fluorescence transitions occur from the lowest excited state S_1, and all other direct transitions $S_n \rightarrow S_0$ are negligible (S_0 and S_n are the ground and a highly excited electronic state, respectively). The excitation anisotropy spectra of **1**, $r(\lambda)$, (Figure 2a, curves 1, 3–5) reveal the nature of the main long-wavelength absorption band. A constant value of anisotropy in the spectral range 380 nm $\leq \lambda_{ex} \leq$ 470 nm corresponds to a single electronic transition $S_0 \rightarrow S_1$, which is responsible for the main absorption band. In viscous polyTHF (pTHF), the maximum fundamental anisotropy value, $r \approx 0.38$, is close to the theoretical limit,[36] which is indicative of nearly parallel orientation of the absorption, $S_0 \rightarrow S_1$, and emission, $S_1 \rightarrow S_0$, transition dipole moments, $\boldsymbol{\mu}_{01}$ and $\boldsymbol{\mu}_{10}$, respectively. Fluorescence emission processes in **1** exhibited a single exponential decay in all of the investigated solvents (Figure 2b), with corresponding lifetimes in the range 1 – 4 ns (Table 1). These values of fluorescence lifetimes, τ, were also calculated as: $\tau_{cal} = \tau_R \cdot \Phi$, where τ_R is the radiative lifetime obtained by the Strickler-Berg equation.[37] An acceptable correlation between experimental τ and calculated, τ_{cal}, lifetimes (presented in Table 1), along with a weak dependence of the steady-state absorption spectra on solvent polarity (Figure 1), are indicative of the absence of the strong specific solute-solvent interaction of **1** in the employed aprotic solvents. In the most polar ACN, a strong decrease in the fluorescence quantum yield was observed, and the experimental value of lifetime could not be determined with acceptable accuracy with the experimental equipment used. The values of rotational correlation time, $\theta \approx$ 190 ps, and the effective rotational volume of **1** in THF, $V \approx 160$ $Å^3$, were estimated from equation 2 (see Experimental Section) based on the assumption of equal values of the fundamental anisotropies, r_0, of **1** in viscous pTHF and nonviscous THF and using fluorescence lifetimes and anisotropy data. The relatively fast rotation and small rotational volume of **1** allow for the assumption of the "in-plane" character of the molecular rotation and slipping boundary conditions in solute-solvent dynamics.[38] The processes of the photochemical decomposition of **1** exhibited the first order of the photochemical reaction in TOL, $CHCl_3$ THF, and ACN, with corresponding quantum yields, Φ_{ph}, in the range of ~ $(1–4) \cdot 10^{-5}$ (Table 1), which is of a sufficiently high level of molecular photostability for its practical applications. In nonpolar HEX, the value of Φ_{ph} dramatically increased, and a complicated photochemical kinetic was observed. Detailed photochemical investigations were beyond the scope of this paper.

Quantum-chemical calculations

The optimized molecular geometry of **1** is presented in Figure 3 and reveals nearly equalized bond lengths of 1.40 ± 0.01 Å in all of the benzene rings, while the lengths of the bonds in the external chain show considerable alternation. As follows from these calculations, both phenyl substituents at the nitrogen atom are turned out at 44°; the rest of the optimized molecular structure is planar and exhibits sufficiently small rotational barriers (~ 2 kcal/mol) between fluorene moiety and whole external substituents. The values of oscillator strengths, f_{OS}, main configurations and transition dipoles $\boldsymbol{\mu}_{ij}$, ($i = 0, 1$; $j = 2, 3, \ldots$) among the first 6 singlet electronic levels S_0, S_1, …, S_5), along with the shape of the corresponding molecular orbitals (MO), are presented in Table 2 and Figure 4, respectively. As follows from the data

$watermark-text

$watermark-text

$watermark-text

in Figure 4, both phenyl substituents of the nitrogen atom do not take part in the LUMO and LUMO+1, whereas the thiophene ring contributes considerably in the lowest vacant MO. At the same time, the highest occupied MOs (HOMO and HOMO-1) are nearly insensitive to such chemical modifications of the fluorene moiety. The local orbital, HOMO-2, includes atoms of the thiophene ring only and does not participate in the main electronic transitions. The first electronic transition is described by one pure configuration and is connected with the long-wavelength band in the linear absorption, which is in good agreement with the steady-state (anisotropy spectrum (Figure 2a, curve 1). The calculated oscillator strength of the second transition ($S_0 \rightarrow S_2$), $f_{OS} \approx 0$, and therefore, this transition cannot be observed in linear absorption. In contrast, the values of the oscillator strengths of the next two transitions $S_0 \rightarrow S_3$ and $S_0 \rightarrow S_4$ are sufficiently large and are comparable with the intensity of the main long-wavelength absorption band, which also reveals good correspondence between the calculated data and the observed short-wavelength absorption contour (Figure 1).

2PA properties of 1

The degenerate 2PA spectra of **1** (Figure 5) were investigated in a broad spectral range (590–1020 nm), in solvents of different polarity by open aperture Z-scan[33] and 2PF[34] methods. A good agreement between the experimental 2PA cross-section values, δ_{2PA}, obtained by two independent nonlinear optical methodologies was observed in the spectral range 660–840 nm. An unsymmetrical compound **1** exhibited two well-defined 2PA bands at $\lambda_{ex} \approx$ 640–680 nm and 880–900 nm, with maximal cross-sections $\delta_{2PA} \approx$ 200–350 GM and 400–600 GM, respectively, and revealed a weak dependence of 2PA efficiency on solvent polarity. The shape of these spectra is typical for unsymmetrical fluorene derivatives,[39, 40] where a relatively strong2PA band overlaps with the main one-photon–allowed long-wavelength absorption contour. The nature of this band can be attributed to the possible changes in the stationary dipole moment of **1**, $\Delta\boldsymbol{\mu}_{01}$, under electronic excitation, $S_0 \rightarrow S_1$, in accordance with the expression, based on simplified three-level model of 2PA processes:[41]

$$\delta_{2PA} = \frac{64\pi^4}{15c^2h^2n^2}\left[\frac{\nu_{ex}^2\left|\boldsymbol{\mu}_{\mathbf{01}}\right|^2\left|\boldsymbol{\mu}_{\mathbf{1}f}\right|^2}{E^2+\Gamma_{01}^2}(1+2\cos^2\alpha)+\left|\Delta\boldsymbol{\mu}_{\mathbf{0}f}\right|^2\left|\boldsymbol{\mu}_{\mathbf{0}f}\right|^2(1+2\cos^2\beta)\right].g(2\nu_{ex}), \quad (1)$$

where $E=hc(1/\lambda_{ab}^{\max}-1/\lambda_{ex})$; $\nu_{ex} = c/\lambda_{ex}$; $\boldsymbol{\mu}_{\mathbf{0}f}$, and $\boldsymbol{\mu}_{1f}$ are the transition dipoles moments for $S_0 \rightarrow S_f$ and $S_1 \rightarrow S_f$ electronic transitions, respectively (S_f is the final electronic state); $\Delta\boldsymbol{\mu}_{\mathbf{0}f} = \boldsymbol{\mu}_{\mathbf{00}} - \boldsymbol{\mu}_{ff}$ is the difference in the stationary dipole moments of the ground and final electronic states, respectively; Γ_{01} is the damping constant related to the transition frequency $\nu_{01}=c/\lambda_{ab}^{\max}$; α and β are the angles between the vectors $\boldsymbol{\mu}_{01}$, $\boldsymbol{\mu}_{1f}$ and $\Delta\boldsymbol{\mu}_{0f}$ $\boldsymbol{\mu}_{0f}$ respectively; $g(2\nu_{ex})$ is the normalized Lorentzian shape function; and n is the refractive index of the medium. Eq. (1) is based on the sum over state (SOS) approach [42] and for 2PA excitation $S_0 \rightarrow S_1$ gives $\delta_{2PA} \sim |\Delta\boldsymbol{\mu}_{\mathbf{01}}|^2 |\boldsymbol{\mu}_{\mathbf{01}}|^2 (1 + 2\cos^2\alpha_2) \cdot g(2\nu_{exc})$. The calculated values of the maximum 2PA cross-sections of **1,** for the most intensive two-photon transitions $S_0 \rightarrow S_1$, $S_0 \rightarrow S_2$, and $S_0 \rightarrow S_4$, are presented in Table 3. These cross-sections were obtained by eq. (1) using corresponding dipole moments from Table 2, calculating change in the stationary dipole moment of **1** under electronic excitation $S_0 \rightarrow S_1$, $\Delta\boldsymbol{\mu}_{01} \approx$ 5.4 D, and damping constant Γ_{01} = 0.1 eV. As follows from the comparison of the experimental and calculated 2PA data, the best agreement is observed for $S_0 \rightarrow S_2$ and $S_0 \rightarrow S_4$ two-photon transitions. The noticeable difference between calculated and experimental 2PA cross-sections for $S_0 \rightarrow S_1$ transition may be of concern with some underestimation of the change in the stationary dipole moments of **1**.

$watermark-text

$watermark-text

$watermark-text

A potential of **1** for practical application in 2PFM can be estimated based on Figure of Merit, $F_M = \Phi \cdot \delta_{2PA}/\Phi_{ph}$, introduced previously in ref.[31] As follows from the data in Tables 1 and 3, the values of F_M for compound **1** can be estimated as ~$10^6 - 6 \cdot 10^7$, which are comparable with the best examples of the 2PA fluorescence labels.[43] High values of F_M make fluorene derivative **1** a promising candidate for 2PFM applications using commercial femtosecond Ti:Sapphire lasers.

One- and two-photon STED spectra of 1

The steady-state and time-resolved STED spectra of **1** were investigated in TOL and $CHCl_3$. A schematic diagram of the main spontaneous and stimulated transitions in **1** that occurred after electronic excitation is depicted in Figure 6. The values of one- and two-photon stimulated emission cross-sections ($\sigma_{10}(\lambda_q)$ and $\sigma_{2PE}(\lambda_q)$, correspondingly) were obtained in a broad spectral range by a fluorescence quenching pump-probe method,[24] using femtosecond laser pulses. In the case of the steady-state STED measurements, a constant value of time delay between pump and probe beam, $\tau_D = 20$ ps $\ll \tau$, was used, assuming that all excited state vibrational and solvate relaxation processes of **1** were finished in 20 ps, and after that, the observed STED spectra should be constant in time. The nature of STED processes for one- and two-photon stimulated emission transitions were determined from the experimental dependences $1 - I_F/I_{F0} \sim \sigma_{10}(\lambda_q) \cdot {}^qE_P$ and $1 - I_F/I_{F0} \sim \delta_{2PE}(\lambda_q) \cdot {}^qE_P^2$, presented in Figures 7a and 7c, respectively (I_F and I_{F0} are the integral fluorescence intensities observed from one excitation pulse in the presence and absence of the quenching beam, correspondingly; λ_q is the quenching wavelength and ${}^qE_P$ is the energy of the quenching pulse). Similar dependences were obtained for each quenching wavelength λ_q. A linear character of these dependences reveals the pure one- and two-photon nature of corresponding stimulated emission processes, occurring in **1** under the employed experimental conditions. The one-photon STED spectra of **1** in TOL and $CHCl_3$ (Figure 7b, curves 3, 4) exhibited maximal cross-sections $\sigma_{10}(\lambda) \sim (5–6) \cdot 10^{-17}$ cm^2 and were sufficiently close to the corresponding steady-state fluorescence contours (curves 1′, 2′). These maxima of $\sigma_{10}(\lambda)$ reveal small long-wavelength shifts ~10–20 nm relative to the maxima of fluorescence spectra, $I_F(\lambda)$, which is in good agreement with the theoretical prediction: $\sigma_{10}(\lambda) \sim \lambda 4 \cdot I_F(\lambda)$.[44] It is worth mentioning that the absolute values of stimulated emission cross-sections $\sigma_{10}(\lambda)$ exhibit sufficiently large deviation from the corresponding ground state absorption cross-sections, $\sigma_{01}(\lambda) \approx (1–1.2) \cdot 10^{-16}$ cm^2 (for **1** in TOL and $CHCl_3$), which could be evidence of a strong influence of the solvate relaxation processes on the shape of the excited-state potential energy of **1**. The two-photon STED spectrum of **1** was obtained only in $CHCl_3$ (Figure 7d, curve 3), where the linear dependences $1 - I_F/I_{F0} \sim \delta_{2PE}(\lambda_q) \cdot {}^qE_p^2$ were observed (Figure 7c). The maximum values of the two-photon stimulated emission cross-sections, $\delta_{2PE}^{max} \approx 400$ GM, were less than the ground-state 2PA cross-sections, $\delta_{2PA}^{max} \approx 600$ GM, and a small short wavelength shift of δ_{2PE}^{max} relative to the steady-state fluorescence contour was observed. It can be assumed that the nature of the two-photon STED spectrum of **1** is similar to the observed long-wavelength band in the 2PA spectrum (Figure 7d, curve 2) and is determined by the product: $\delta_{2PE}^{max} \sim |\boldsymbol{\mu}_{10}|^2 \cdot |\Delta\boldsymbol{\mu}_{10}|^2$, where $\boldsymbol{\mu}_{10} \sim \int_{\lambda} \sigma_{10}(\lambda) d\lambda$ is the transition dipole of stimulated emission $S_1 \rightarrow S_0$ and $\Delta\boldsymbol{\mu}_{10}$ is the change in the corresponding stationary dipole moments of S_1 and S_0 electronic states, respectively. In TOL solution of **1,** the efficiency of two-photon stimulated emission processes was not determined by the fluorescence quenching method due to the extremely low degree of two-photon fluorescence quenching. This result is not completely understandable and may be concerned with efficient ground-state three-photon absorption at ~1300 nm, which, in part, compensates for fluorescence quenching processes.

$watermark-text

$watermark-text

$watermark-text

The time-resolved one-photon STED spectra of **1** were determined from the transient quenching efficiency curves, $1 - I_F/I_{F0} = f(\tau_D)$ (Figure 8a, c), obtained for different λ_q, and presented in Figure 8b, d. As follows from these data, the degree of fluorescence quenching decreases with time for short quenching wavelength, $\lambda_q < \lambda_{em}^{max}$, and increases for $\lambda_q > \lambda_{em}^{max}$ in the picosecond time scale. This finding means a possibility exists to reveal instantaneous stimulated emission contours, $\sigma_{10}(\lambda)$, which reflect picosecond solvate relaxation processes. Time-resolved one-photon STED spectra of **1** exhibit maximal long-wavelength shifts up to ~15–20 nm, with corresponding relaxation time ~5–7 ps, which are typical for the solvate relaxation processes of organic molecules in low-viscosity solvents at room temperature.[36] It should be mentioned that the femtosecond fluorescence quenching method is the most accurate methodology for the determination of the molecular stimulated-emission cross-sections, which are important parameters for STED microscopy applications. At the same time, high-intensity femtosecond laser pulses cannot realize more than ~50 % depopulation of the excited state S_1 due to a short pulse duration $\tau_q \ll \tau_V$ (τ_V is the vibrational relaxation time in S_0). This finding means that nano- and picosecond laser pulses are more preferable for the development of high-resolution STED microscopy systems.[45]

One- and two-photon bioimaging

We previously demonstrated that encapsulation of hydrophobic 2PA probes in Pluronic® F-127 is a feasible method for delivering fluorescent probes into the lysosomes of HCT 116 cells.[46, 47] Pluronic® F-127 is a nonionic, surfactant polyol (molecular weight approximately 12,500 daltons) that has been found to facilitate the solubilization of water-insoluble dyes and other materials in physiological media.[48] Probe **1** was encapsulated in Pluronic® F-127, and upon formation of micelles was incubated with HCT 116 cells. In order to demonstrate the potential utility of probe **1** for 2PFM cellular imaging, its cell viability was evaluated. Viability assays in an epithelial colorectal carcinoma cell line, HCT 116, were conducted via the MTS assay (Figure S1 shows the viability data for HCT 116 cells after treatment with several concentrations of dye-encapsulated micelles for 24 h). The data indicate that probe **1** has low cytotoxicity (~ 95% viability) over a concentration range from 1 to 30 μM, appropriate for cell imaging. To determine the location of the probe **1** in the cell, a colocalization study of probe **1** with well-known lysosomal selective dye (Lysotracker Red) in HCT 116 cells was conducted. One-photon fluorescence images, collected for Lysotracker Red and probe **1**, are shown in Figure 9b and c, respectively, as well as the differential interference contrast (DIC) image (Figure 9a), along with the overlap image of a, b, and c (Figure 9d). One can observe in Figure 9d, the colocalization of both probes suggesting a similar uptake mechanism for both the Lysotracker dye and probe **1**. Pearson's correlation coefficient was calculated within Slidebook 5.0, imaging processing software. The correlation coefficient of probe **1** relative to LysoTrackerRed is higher than 0.8, supporting lysosomal colocalization. 2PFM imaging (Figure 10c) revealed remarkable contrast when compared to the one-photon fluorescence (Figure 10b), suggesting the potential that this probe-micelle formulation has in bioimaging.

Conclusion

The synthesis, linear photophysical, and nonlinear optical properties of new push-pull fluorene derivative **1,** with a strong electron-donor di-*p*-tolylamine group and electron-acceptor acetylthiophene, were investigated in a number of organic solvents at room temperature as a potential fluorescent label for 2PFM applications. The steady-state absorption spectra of **1** exhibited weak dependence on solvent properties, while fluorescence emission revealed strong solvatochromic behavior with a maximum Stokes shift of more than 180 nm in $CHCl_3$. The values of fluorescence quantum yields of **1** in different media are high (~0.6–1.0) and independent of excitation wavelength in a whole spectral range of

$watermark-text

$watermark-text

$watermark-text

absorption. Fluorescence lifetimes corresponded to a single exponential decay and were in good agreement with theoretical predictions, based on the Strickler-Berg approach. The excitation anisotropy spectra of **1** revealed only one electronic transition $S_0 \rightarrow S_1$ in the main long-wavelength absorption band, relatively fast rotational correlation time in low-viscosity solvents, $\theta \approx 190$ ps, and small effective rotational molecular volume $V \approx 160$ Å^3, which could be associated with slipping boundary conditions in solute-solvent dynamics. The degenerate 2PA spectra of **1** were obtained by two independent methods and exhibited two well-defined 2PA bands. The strongest one was observed in the spectral range $\lambda_{ex} \approx$ 880–900 nm with maximal cross-sections $\delta_{2PA} \approx$ 400–600 GM and corresponded to the linear long-wavelength absorption contour. That is suitable for practical applications of **1** in 2PFM with commercially available femtosecond Ti:sapphire laser systems.

The electronic structure of **1** was analyzed based on the results of TDDFT quantum-chemical calculations, and the nature of the main electronic transitions responsible for linear and nonlinear optical properties was determined. The steady-state one- and two-photon stimulated emission spectra of **1** were obtained over a broad spectral region and a maximum two-photon cross section $\delta_{2PE} \approx$ 400 GM was shown. This value is close to the corresponding ground-state 2PA cross-sections in the main linear absorption band of **1**, which presumably reflects the two-photon nature of these processes. The time-resolved one-photon STED spectra were obtained for the first time using a femtosecond fluorescence quenching method. The spectral shifts of the stimulated emission contours, $\sigma_{10}(\lambda)$, up to 20 nm, were observed within a time period of 5–7 ps due to the solvate relaxation processes. It seems that the presented fluorescence quenching methodology is a promising and relatively simple way of estimating the time-resolved fluorescence spectra of organic molecules. The potential application of **1** in bioimaging was demonstrated via one- and two-photon fluorescence microscopy of epithelial colorectal carcinoma HCT 116 cells encapsulated in Pluronic® F-127 micelles. Based on these results, a new fluorene derivative **1,** exhibiting relatively large 2PA and two-photon stimulated emission cross-sections, high-fluorescence quantum yield, and photochemical stability, has good potential for 2PFM applications as a fluorescent label, including STED bioimaging microscopy.

Experimental Section

Materials and synthetic methods

We report the preparation of a new push-pull fluorene derivative bearing a strong electron-donor di-*p*-tolylamine group and acetylthiophene as an electron acceptor. The preparation of the push-pull compound **1** was carried out using commercially available 1-(thiophen-2-yl)ethanone (**B**) and aldehyde derivative **A**, as shown in Scheme 1. Claisen-Schmidt condensation was performed in MeOH and KOH under reflux-affording compound 1 in 45% yield. The analysis of the ^{1}H- and ^{13}C-NMR spectra confirmed the expected molecule. Synthesis of 7-(di-*p*-tolylamino)-9,9-diethyl-9H-fluorene-2-carbaldehyde (**A**) will be described elsewhere. 1-(Thiophen-2-yl)ethanone (**B**) was commercially available. The ^{1}H and ^{13}C NMR measurements were performed using a Varian 500 NMR spectrometer at 500 MHz with tetramethysilane (TMS) as the internal reference. For ^{1}H (referenced to TMS at δ = 0.0 ppm) and for ^{13}C (referenced to $CDCl_3$ at δ = 77.0 ppm), the chemical shifts of ^{1}H and ^{13}C spectra were interpreted with the support of CS ChemDraw Ultra, version 11.0. High-resolution mass spectrometry (HR-MS) analysis was performed in the Department of Chemistry, University of Florida, Gainesville, FL.

Synthesis of (E)-1-(2-(di-p-tolylamino)-9,9-diethyl-9H-fluoren-7-yl)-3-(thiophen-2-yl)prop-2-en-1-one (1)—1-(Thiophen-2-yl)ethanone (0.14 g, 1.12 mmol) was added to the solution of KOH (0.075 g, 1.34 mmol) in MeOH/H_2O 5:1 (20 mL). After

$watermark-text

$watermark-text

$watermark-text

dissolution 7-(di-*p*-tolylamino)-9,9-diethyl-9H-fluorene-2 carbaldehyde (0.50 g, 1.12 mmol) was added to the mixture and stirred for 48 h at reflux. A solid-product precipitate was filtered, washed with hexane, and dried. Recrystallization in hexanes provided yellow solid 0.27 g (45% yield), m.p. 172–173 °C, ^{1}H NMR (500 MHz, $CDCl_3$) δ: 7.95 (s, 1H), 7.92 (t, J = 5.5 Hz, 2H), 7.68 (d, J = 5Hz, 1H), 7.61 (s, 2H), 7.54 (t, J = 8.5 Hz, 2H)7.45 (d, J = 15.5 Hz, 1H), 7.20 (t, J =5 Hz, 1H), 7.06-7.01 (m, 8H), 6.98 (dd, J = 8 Hz, 1H), 2.32 (s, 6H), 2.01-1.88 (m, 4H), .382-0352 (t, J = 15 Hz, 6H). ^{13}C NMR (500 MHz, $CDCl_3$) δ: 182.1, 152.0, 150.4, 148.6, 145.8, 145.4, 145.0, 144.6, 134.4, 133.5, 132.5, 132.4, 131.5, 129.8, 128.3, 128.1, 124.4, 122.6, 122.0, 120.8, 119.9, 119.2, 117.4, 56.0, 32.6, 20.8, 8.5 ppm. HRMS-ESI theoretical m/z $[M+H]^+$ = 554.24, found 554.25, theoretical m/z $[M+Na]^+$ = 576.24, found 576.23.

Linear photophysical and photochemical characterization

The linear steady-state absorption, excitation, fluorescence, and excitation anisotropy spectra of **1** were investigated in spectroscopic grade HEX, TOL, $CHCl_3$, THF and ACN at room temperature. The steady-state absorption measurements were carried out using an Agilent 8453 UV-visible spectrophotometer and 10-mm path length quartz cuvettes with dye concentrations C ~ (2–4) · 10^{-5} M. The steady-state excitation, fluorescence, and excitation anisotropy spectra were obtained with a PTI QuantaMaster spectrofluorimeter in a photon-counting regime using 10-mm spectrofluorometric quartz cuvettes with C ≤ 10^{-6} M. All excitation and fluorescence spectra were corrected for the spectral responsivity of the PTI excitation and detection system, respectively. Excitation anisotropy measurements were performed in the "L-format" configuration,[36] and a weak emission of pure solvent and scattered light were extracted. The fundamental anisotropy value of **1** r_0, was determined in viscous pTHF, in which the rotational correlation time, $\theta = \eta V/(kT) \gg \tau$ (τ, V, k, and T are the viscosity of solvent, effective rotational molecular volume, Boltzmann's constant, and absolute temperature, respectively) and experimentally observed anisotropy:[36]

$$r = r_0/(1+\tau/\theta) \approx r_0, \quad (2)$$

The values of fluorescence quantum yields, Φ, of **1** were determined in low concentrated solutions (C ~ 10^{-6} M) by a standard relative method with 9,10-diphenylanthracene in cyclohexane as a reference (Φ ≈ 0.95).[36] Fluorescence lifetimes of **1**, τ, were obtained using a time-correlated single-photon counting PicoHarp 300 system with time resolution ≈ 80 ps. Linear polarized femtosecond excitation, oriented by the magic angle, was used in the lifetime measurements to avoid the effect of rotational molecular movement on τ. The quantum yields of the photochemical decomposition of **1**, Φ_{ph}, were determined under cw one-photon excitation with a LOCTITE 97034 UV lamp (excitation wavelength, λ_{ex} ≈ 405 nm, average irradiance ≈ 90 mW/cm^2) by the absorption method described previously.[49]

2PA and STED measurements

The investigations of the 2PA and STED properties of **1** were performed with a femtosecond laser system (Coherent, Inc.), schematically depicted in Figure 11. The output of a Ti:Sapphire laser (Mira 900-F, tuned to 800 nm, with a repetition rate, f = 76 MHz, average power ≈ 1.1 W and pulse duration, τ ≈ 200 fs), pumped by the second harmonic of cw Nd^{3+}:YAG laser (Verdi-10), was regeneratively amplified with a 1-kHz repetition rate (Legent Elite USP) providing ≈ 100 fs pulses (FWHM) with energy ≈ 3.6 mJ/pulse. This output at 800 nm was split in two separate beams with average power ≈ 1.8 W each and pumped two ultrafast optical parametric amplifiers (OPerA Solo (OPA), Coherent Inc.) with a tuning range 0.24-20 μm, τ_P ≈ 100 fs (FWHM), and pulse energies, E_P, up to ≈ 100 μJ. A single laser beam from the first OPA was used for direct 2PA cross-section measurements

$watermark-text

$watermark-text

$watermark-text

by the open-aperture Z-scan method.[33] The same laser exit was coupled with a PTI QuantaMaster spectrofluorimeter (this part is not shown in Figure 11), and the relative 2PF method[34] was used for 2PA measurements, as well as Rhodamine B in methanol and fluorescein in water (pH=11) as standards.[50] The quadratic dependence of 2PF intensity on the excitation power was confirmed for each excitation wavelength, λ_{ex}. The investigation of the steady-state and time-resolved STED spectra of **1** were performed based on the pump-probe fluorescence quenching technique,[24] using two laser beams from the separate OPA systems simultaneously pumped at 800 nm (Figure 11). The fluorescence quenching method is based on one- or two-photon stimulated emission transitions $S_1 \rightarrow S_0$ (S_0 and S_1 are the ground and first excited electronic states of **1**, respectively), which can depopulate electronic state S_1 (after a short time delay, $\tau_D \ll \tau$, following the excitation) and decrease the fluorescence intensity observed perpendicular to the excitation beam. The first (pump) beam from OPA was set at 400 nm ($\tau_P \approx 100$ fs; $f = 1$ kHz; $E_P \approx 1$ μJ) and was used for one-photon fluorescence excitation of **1**. The second (quenching) beam from another OPA was delayed by a M-531.DD optical line with a retroreflector and was tuned in a broad spectral range (quenching wavelengths 440 nm $\leq \lambda_q \leq$ 1600 nm; quenching pulse duration, $\tau_q \approx 100$ fs; $f = 1$ kHz; quenching pulse energies, 0.5 μJ $\leq {}^qE_P \leq 8$ μJ). The integral fluorescence intensities from the investigated solutions of **1** were observed perpendicularly to the excitation beam and were measured with an H4000 fiber optic spectrometer (Ocean Optics Inc.). In the case of one-photon STED transitions (λ_q belongs to the fluorescence region of **1**), the pumping and quenching laser beams, with vertically oriented linear polarizations, were focused on the waists of the radiuses ${}^pr_0 \approx 0.5$ mm and ${}^qr_0 \approx 0.2$ mm (HW1/eM), respectively, and were recombined at a small angle (< 5°) in a 1-mm path length flow quartz cuvette with a sample solution. Two-photon STED transitions ($\lambda_q/2$ belongs to the fluorescence region of **1**) were realized in a similar excitation and quenching geometry with ${}^pr_0 \approx 0.18$ mm and ${}^qr_0 \approx 0.1$ mm (HW1/eM), respectively. The optimum optical density of the investigated solutions at λ_{ex} was in the range 0.3 – 0.4. The efficiency of the fluorescence quenching processes is characterized by the degree of fluorescence quenching, $1 - I_F/I_{F0}$, where I_F and I_{F0} are the integral fluorescence intensity observed from one excitation pulse in the presence and absence of the quenching beam, respectively. In the case of one-photon quenching, this value can be expressed as:[14]

$$1-I_F/I_{F0}=\frac{2\cdot\lambda_q\cdot\sigma_{10}(\lambda_q)}{\pi\cdot h\cdot c\cdot({}^pr_0^2+{}^qr_0^2)}\cdot{}^qE_P, \quad (3)$$

where $\sigma_{10}(\lambda_q)$, h, c are the one-photon stimulated emission cross-section at λ_q, Planck's constant, and velocity of light in a vacuum, respectively. In the case of the two-photon fluorescence-quenching process, equation (3) can be written as:[14]

$$1-I_F/I_{F0}=(8/\pi^5)^{1/2}\cdot\frac{\lambda_q^2\cdot\delta_{2PE}(\lambda_q)}{h^2\cdot c^2\cdot(2\cdot{}^pr_0^2+{}^qr_0^2)}.{}^qE_P^2, \quad (4)$$

where $\delta_{2PE}(\lambda_q)$ is the two-photon stimulated emission cross-section at λ_q. Equations (3) and (4) were obtained under several reasonable approximations that corresponded to the employed experimental conditions (Gaussian spatial and temporal shapes of the pumping and quenching beams; constant field approximation; spectral independence of the fluorescence quantum yield of **1**; sufficiently high photochemical stability of the investigated solutions, etc.) and described previously in detail.[14] The slopes of the linear experimental dependences $1 - I_F/I_{F0} \sim \sigma_{10}(\lambda_q)\cdot{}^qE_P$ and $1-I_F/I_{F0}\sim\delta_{2PE}(\lambda_q)\cdot{}^qE_P^2$ were used for the determination of the $\sigma_{10}(\lambda_q)$ and $\delta_{2PE}(\lambda_q)$ cross-sections. It should be mentioned

$watermark-text

$watermark-text

$watermark-text

that the linearity of these dependences can serve as a proof of the one- or two-photon nature of the observed STED processes and was confirmed for each excitation wavelength. Also, it is important to emphasize that one-photon excited state absorption (ESA) processes cannot affect the efficiency of fluorescence quenching in cases in which the value of the fluorescence quantum yield is independent of the excitation wavelength. This means that direct radiationless transitions from highly excited electronic states to S_0 are negligible, and additional ESA processes cannot decrease fluorescence intensity. The steady-state one- and two-photon STED spectra of **1** were obtained for the constant value of τ_D = 20 ps, which is an optimal time delay for the investigation of organic molecules with nanosecond fluorescence lifetimes.[14, 24] It was reasonable to assume that a negligible amount of fluorescence photons were emitted in the time period of 20 ps after excitation, and all excited state vibrational and solvate relaxation processes in **1** were finished.[36] The time-resolved STED spectra of **1** were obtained for one-photon stimulated emission transition by tuning of λ_q in the fluorescence spectral range and for a varied time delay between the pump and quench pulses in the range 0 – 20 ps. The time-resolution of the used experimental setup was approximately 300 fs. Typical dependence $1 - I_F/I_{F0} = f(\tau_D)$, determining the time resolution of this system, is shown in Figure 12, with the step in $\tau_D \approx 6.7$ fs. It should be mentioned that no photochemical or other accumulative effects were observed in the flow sample solutions under the experimental conditions.

Computational details

Quantum-chemical calculations of the electronic structure of **1** were performed with the Gaussian 09 program package.[35] The ground state geometry was optimized by the DFT/6–31(d,p)/B3LYP method. The time-dependent density functional theory (TDDFT/6–31(d,p)/B3LYP) was employed to obtain molecular orbitals, excitation energies, oscillator strengths, and steady-state and transition dipoles for the optimized structure. The values of 2PA cross-sections were estimated by the well-known expression of Ohta et al.,[41] based on the SOS approach and the simplified three-level model of 2PA processes.[42]

Preparation methodologies of dye-encapsulated micelles, cell incubation and fluorescence bioimaging

Encapsulation of probe 1 in Pluronic® F-127—A solution containing 12.5 mg of Pluronic® F-127 in 5mL of PBS buffer (pH= 7.4) was mixed with a solution containing dye **1** (2.5 mg) in CH_2Cl_2 (5 mL). The resulting mixture was stirred at room temperature for 48 h to slowly evaporate the CH_2Cl_2. The mixture was filtered through a Whatman 2 μm pore size disposable filter to generate stock solution. The concentration of stock solution was 252 μM, estimated by absorption spectra.

Cell culture and incubation—HCT 116 cell (purchased from America Type Culture Collection, Manassas, VA) were cultured in RPMI-1640, supplemented with 10% FBS, and 1% peniclin, 1% streptomycin, at 37 °C, in a 95% humidified atmosphere containing 5% CO_2. N° 1 round 12 mm coverslips were treated with poly-D-lysine, to improve cell adhesion, and washed (3×) with PBS buffer solution. The treated cover slips were placed in 24-well plates and 40,000 cells/well were seeded and incubated for 36 h before incubation with the dye. From a 252 μM stock solution of Pluronic® F-127 encapsulated dye **1** a 20 μM solution in culture media was freshly prepared and also a 75 nM solution of Lysotracker Red (Invitrogen). These solutions were used to incubate the cells for 1 h. After incubation, cells were washed with PBS three times, fixed with 3.7% formaldehyde in PBS at room temperature for 10 min, and incubated twice with $NaBH_4$ (1mg/mL) in PBS at room temperature for 10 min. The cells were then washed with PBS twice and mounted on microscopy slides with Prolong Gold (Invitrogen) mounting media for imaging.

One-photon and two-photon fluorescence imaging—One- and two-photon images were recorded on a Leica TCS SP5 II laser-scanning confocal microscope system. For one-photon imaging, cells were excited at 405 nm. Fluorescence was collected in a range from 450 nm to 550 nm. The confocal pinhole was applied for better image quality. Two-photon fluorescence imaging was recorded on Leica TCS SP5 microscope system coupled to a tunable Coherent Chameleon Vision S laser (80 MHz, modelocked, 75 fs pulse width, tuned to 700 nm). Two-photon induced fluorescence was collected with a water immersion 63x objective (HCX Pl APO CS 63.0×1.20 WATER UV).

Supplementary Material

Refer to Web version on PubMed Central for supplementary material.

Acknowledgments

We wish to acknowledge the Institute of Bioimaging and Bioengineering of the National Institutes of Health (1 R15 EB008858-01), the National Academy of Sciences of Ukraine (grant 1.4.1.B/153), the National Science Foundation (ECCS-0925712, CHE-0840431, and CHE-0832622), and the National Academy of Sciences (PGA-P210877) for their support of this work.

References

1. Kawata S, Kawata Y. Chem Rev. 2000; 100:1777–1788. [PubMed: 11777420]
2. Yanez CO, Andrade CD, Yao S, Luchita G, Bondar MV, Belfield KD. Appl Mater Interf. 2009; 1:2219–2229.
3. Mendonca CR, Correa DS, Marlow F, Voss T, Tayalia P, Mazur E. Appl Phys Lett. 2009; 95:113309/113301–113303.
4. Corredor CC, Huang ZL, Belfield KD, Morales AR, Bondar MV. Chem Mater. 2007; 19:5165–5173.
5. Ding JB, Takasaki KT, Sabatini BL. Neuron. 2009; 63:429–437. [PubMed: 19709626]
6. Moneron G, Hell SW. Opti Express. 2009; 17:14567–14573.
7. Lin TC, Chen YF, Hu CL, Hsu CS. J Mater Chem. 2009; 19:7075–7080.
8. Charlot M, Izard N, Mongin O, Riehl D, Blanchard-Desce M. Chem Phys Lett. 2006; 417:297–302.
9. Reisner DE, Field RW, Kinsey JL, Dai HL. J Chem Phys. 1984; 80:5968–5978.
10. Lattante S, Barbarella G, Favaretto L, Gigli G, Cingolani R, Anni M. Appl Phys Lett. 2006; 89
11. Kobayashi T, Savatier JB, Jordan G, Blau WJ, Suzuki Y, Kaino T. Appl Phys Lett. 2004; 85:185–187.
12. Bulygin AD, Bykova EE, Zemlyanov AA, Zemlyanov AA. Russian Physics Journal. 2009; 52:862–870.
13. Rebane A, Drobizhev M, Makarov NS, Beuerman E, Zhao Y, Spangler CW. Proc SPIE. 2010; 7599:75990W/75991–75912.
14. Belfield KD, Bondar MV, Yanez CO, Hernandez FE, Przhonska OV. J Phys Chem B. 2009; 113:7101–7106. [PubMed: 19388691]
15. Hales JM, Matichak J, Barlow S, Ohira S, Yesudas K, Brédas JL, Perry JW, Marder SR. Science. 2010; 327:1485–1488. [PubMed: 20167746]
16. He GS, Tan LS, Zheng Q, Prasad PN. Chem Rev. 2008; 108:1245–1330. [PubMed: 18361528]
17. Rumi M, Perry JW. Adv Opt Photon. 2010; 2:451–518.
18. Wildanger D, Rittweger E, Kastrup L, Hell SW. Opt Express. 2008; 16:9614–9621. [PubMed: 18575529]
19. Liu W, Niu H. Phys Rev. 2011; A 83:023830/023831–023835.
20. Kusba J, Lakowicz JR. J Chem Phys. 1999; 111:89–99.
21. Lakowicz JR, Gryczynski I, Kusba J, Bogdanov V. Photochem Photobiol. 1994; 60:546–562. [PubMed: 7870760]

$watermark-text
$watermark-text
$watermark-text

$watermark-text
$watermark-text
$watermark-text

22. Gryczynski IK, Gryczynski J, Malak Z, Lakowicz H, JR. J Fluoresc. 1998; 8:253–261.
23. Gryczynski IBV, Lakowicz JR. J Fluoresc. 1993; 3:85–92.
24. Belfield KD, Bondar MV, Morales AR, Padilha LA, Przhonska OV, Wang X. ChemPhysChem. 2011; 12:2755–2762. [PubMed: 21858908]
25. Blom H, Rönnlund D, Scott L, Spicarova Z, Widengren J, Bondar A, Aperia A, Brismar H. BMC Neuroscience. 2011; 12:16, 1–7. [PubMed: 21272290]
26. Nagerl UV, Bonhoeffer T. J Neurosci. 2010; 30:9341–9346. [PubMed: 20631162]
27. Hao F, Zhang X, Tian Y, Zhou H, Li L, Wu J, Zhang S, Yang J, Jin B, Tao X, Zhou G, Jiang M. J Mater Chem. 2009; 19:9163–9169.
28. Abbotto A, Beverina L, Bozio R, Bradamante S, Ferrante C, Pagani GA, Signorini R. Adv Mater. 2000; 12:1963–1967.
29. Belfield KD, Bondar MV, Hernandez FE, Przhonska OV, Wang X, Yao S. PhysChemChemPhys. 2011; 13:4303–4310.
30. Belfield KD, Andrade CD, Yanez CO, Bondar MV, Hernandez FE, Przhonska OV. J Phys Chem B. 2010; 114:14087–14095. [PubMed: 20949957]
31. Wang X, Nguyen DM, Yanez CO, Rodriguez L, Ahn HY, Bondar MV, Belfield KD. J Am Chem Soc. 2010; 132:12237–12239. [PubMed: 20712313]
32. Pawlicki M, Collins HA, Denning RG, Anderson HL. Angew Chem Int Ed. 2009; 48:3244–3266.
33. Sheik-Bahae M, Said AA, Wei TH, Hagan DJ, Van Stryland EW. IEEE J Quantum Electron. 1990; 26:760–769.
34. Xu C, Webb WW. J Opt Soc Am B. 1996; 13:481–491.
35. Frisch, MJ.; Trucks, GW.; Schlegel, HB.; Scuseria, GE.; Robb, MA.; Cheeseman, JR.; Scalmani, G.; Barone, V.; Mennucci, B.; Petersson, GA.; Nakatsuji, H.; Caricato, M.; Li, X.; Hratchian, HP.; Izmaylov, AF.; Bloino, J.; Zheng, G.; Sonnenberg, JL.; Hada, M.; Ehara, M.; Toyota, K.; Fukuda, R.; Hasegawa, J.; Ishida, M.; Nakajima, T.; Honda, Y.; Kitao, O.; Nakai, H.; Vreven, T.; Montgomery, J.; JA; Peralta, JE.; Ogliaro, F.; Bearpark, M.; Heyd, JJ.; Brothers, E.; Kudin, KN.; Staroverov, VN.; Kobayashi, R.; Normand, J.; Raghavachari, K.; Rendell, A.; Burant, JC.; Iyengar, SS.; Tomasi, J.; Cossi, M.; Rega, N.; Millam, NJ.; Klene, M.; Knox, JE.; Cross, JB.; Bakken, V.; Adamo, C.; Jaramillo, J.; Gomperts, R.; Stratmann, RE.; Yazyev, O.; Austin, AJ.; Cammi, R.; Pomelli, C.; Ochterski, JW.; Martin, RL.; Morokuma, K.; Zakrzewski, VG.; Voth, GA.; Salvador, P.; Dannenberg, JJ.; Dapprich, S.; Daniels, AD.; Farkas, Ö.; Foresman, JB.; Ortiz, JV.; Cioslowski, J.; Fox, DJ. Gaussian 09, Revision A.2. Gaussian, Inc; Wallingford CT: 2009.
36. Lakowicz, JR. Principles of fluorescence spectroscopy. Kluwer; New York: 1999.
37. Strickler SJ, Berg RA. J Chem Phys. 1962; 3:814–822.
38. Hu C, Zwanzig R. J Chem Phys. 1974; 60:4354–4357.
39. Morales AR, Schafer-Hales KJ, Yanez CO, Bondar MV, Przhonska OV, Marcus AI, Belfield KD. ChemPhysChem. 2009; 10:2073–2081. [PubMed: 19449363]
40. Belfield KD, Bondar MV, Frazer A, Morales AR, Kachkovsky OD, Mikhailov IA, Masunov AE, Przhonska OV. J Phys Chem B. 2010; 114:9313–9321. [PubMed: 20590077]
41. Ohta K, Antonov L, Yamada S, Kamada K. J Chem Phys. 2007; 127:084501–084512. [PubMed: 17764263]
42. Orr BJ, Ward JF. Molecular Physics. 1971; 20:513–526.
43. Wang X, Nguyen DM, Yanez CO, Rodriguez L, Ahn HY, Bondar MV, Belfield KD. Biomed Opt Express. 2010; 1:453–462. [PubMed: 21258480]
44. Deshpande AV, Beidoun A, Penzkofer A, Wagenblast G. Chem Phys. 1990; 142:123–131.
45. Leutenegger M, Eggeling C, Hell SW. Opt Express. 2010; 18:26417–26429. [PubMed: 21164992]
46. Yao S, Ahn HY, Wang XH, Fu J, Van Stryland EW, Hagan DJ, Belfield KD. J Org Chem. 2010; 75:3965–3974. [PubMed: 20481577]
47. Andrade CD, Yanez CO, Qaddoura MA, Wang X, Arnett CL, Coombs SA, Bassiouni R, Bondar MV, Belfield KD. J Fluoresc. 2011; 21:1223–1230. [PubMed: 21243414]
48. Lemaster JJ, Trollinger DR, QT, Cascio WE, Ohata H. Methods Enzymol. 1999; 302:341–356. [PubMed: 12876784]

49. Corredor CC, Belfield KD, Bondar MV, Przhonska OV, Hernandez FE, Kachkovsky OD. J Photochem Photobiol C. 2006; 184:177–183.
50. Makarov NS, Drobizhev M, Rebane A. Opt Express. 2008; 16:4029–4047. [PubMed: 18542501]

$watermark-text
$watermark-text
$watermark-text

$watermark-text
$watermark-text
$watermark-text

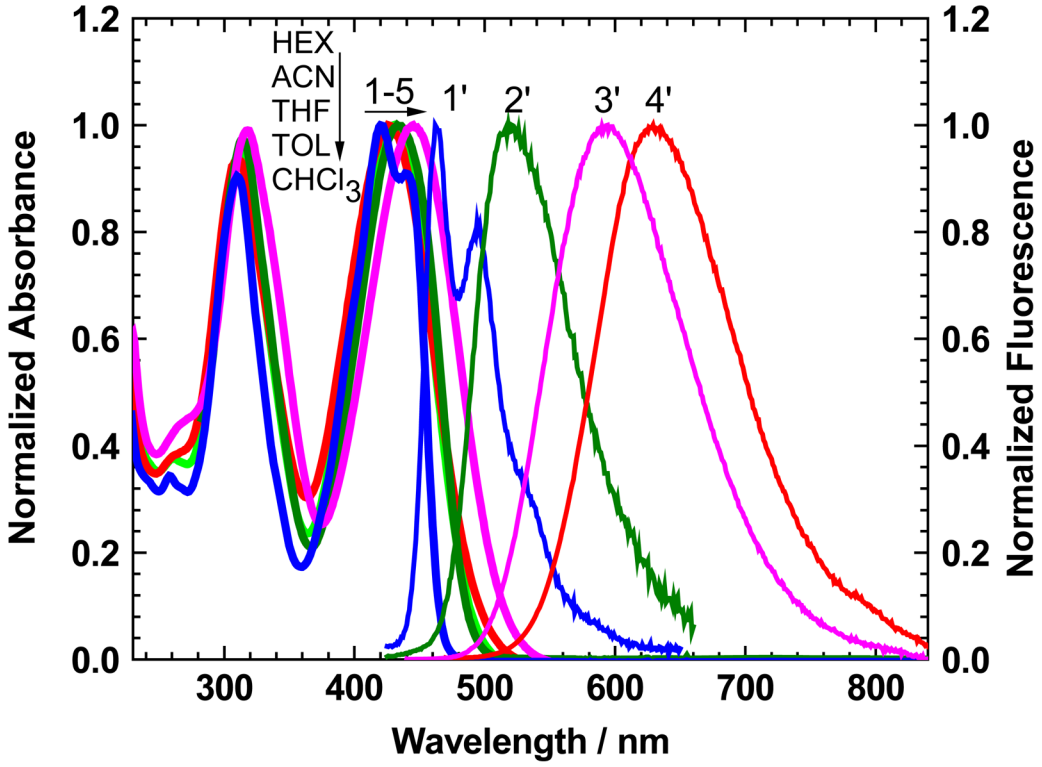

Figure 1.
Normalized steady-state absorption (1–5) and fluorescence (1′-4′) spectra of **1** in HEX (1, 1′), TOL (4, 2′), $CHCl_3$ (5, 4′), THF (3, 3′), and ACN (2).

$watermark-text
$watermark-text
$watermark-text

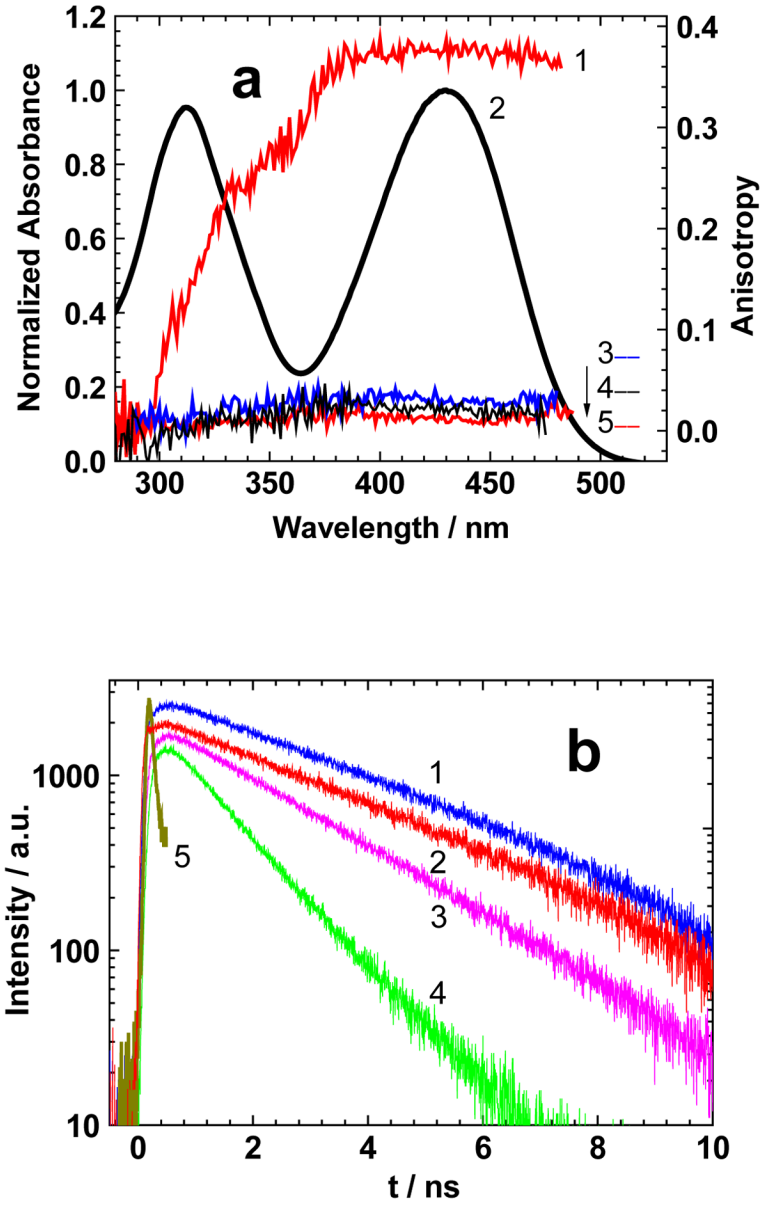

Figure 2.

(a) Excitation anisotropy spectra of **1** in pTHF (1), THF (5), TOL (3), HEX (4), and normalized absorbance in THF (2). (b) Fluorescence lifetime decay curves for **1** in THF (1), $CHCl_3$ (2), TOL (3), HEX (4), and Instrument Response Function (5).

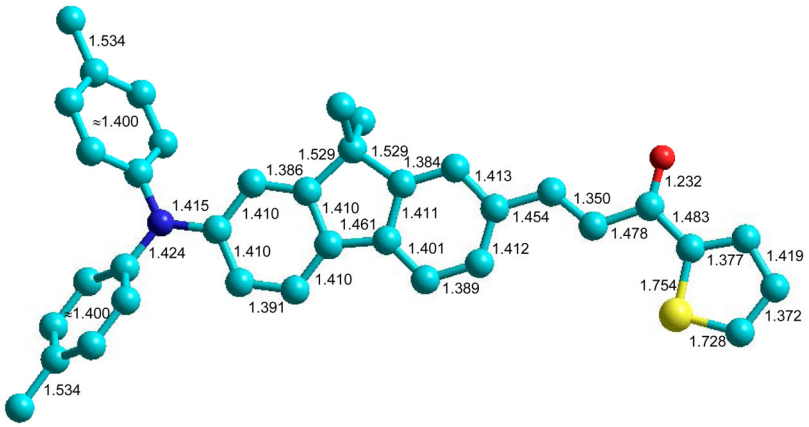

Figure 3.

Optimized molecular geometry of **1** obtained with the DFT/6–31(d,p)/B3LYP method (bond lengths in Å). Ethyl groups are replaced with CH_3 for simplicity.

$watermark-text
$watermark-text
$watermark-text

$watermark-text
$watermark-text
$watermark-text

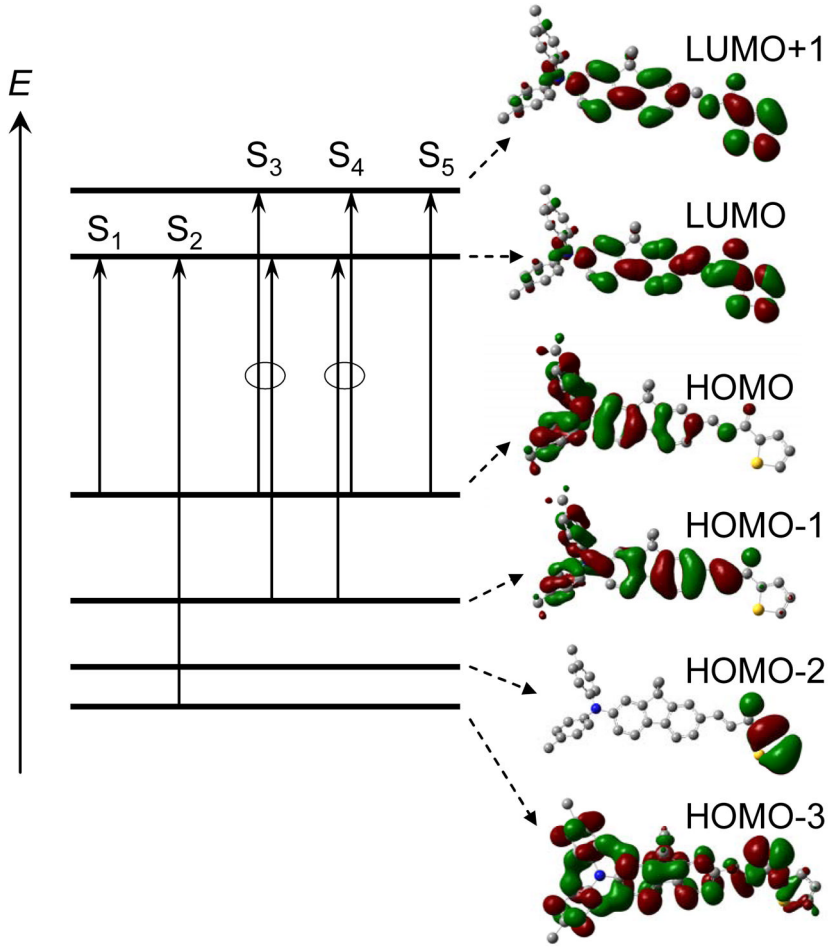

Figure 4.
Main electronic transitions and corresponding molecular orbitals of **1**.

$watermark-text
$watermark-text
$watermark-text

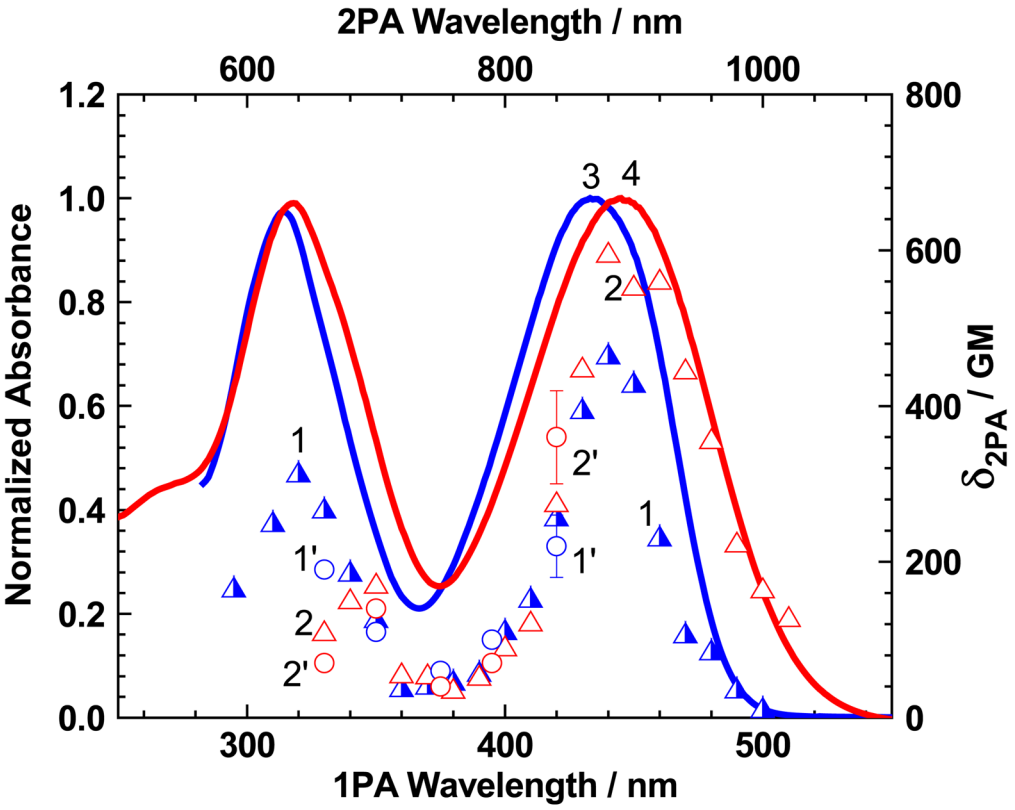

Figure 5.

Degenerate 2PA spectra of 1 in TOL (1, 1′) and $CHCl_3$ (2, 2′), obtained by 2PF (1, 2 - triangles) and open-aperture Z-scan (1′, 2′ - circles) methods. Normalized linear absorption spectra of 1 in TOL (3) and $CHCl_3$ (4).

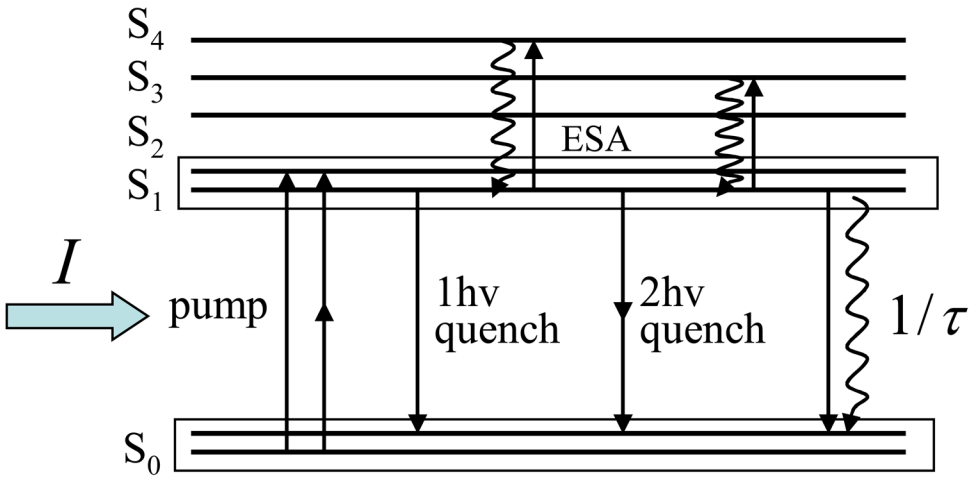

Figure 6.
Schematic diagram of the main spontaneous and stimulated transitions in **1**.

$watermark-text
$watermark-text
$watermark-text

$watermark-text

$watermark-text

$watermark-text

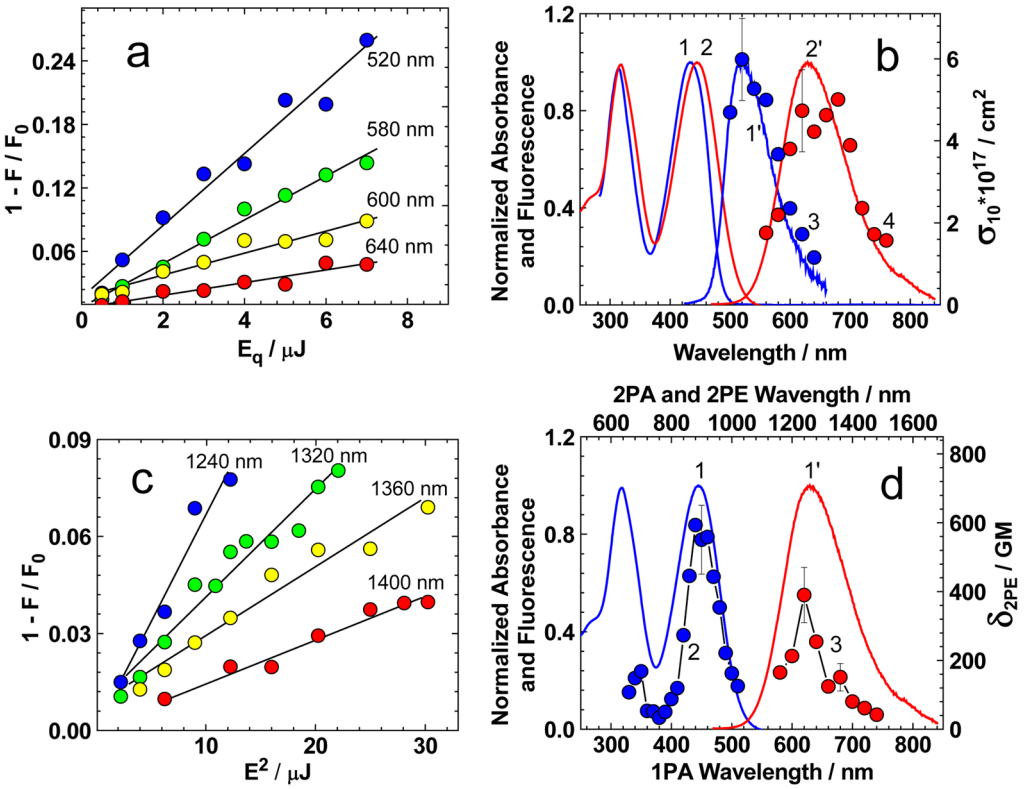

Figure 7.

Fluorescence quenching dependences $1 - I_F/I_{F0} = f(^qE_P)$ (a) and $1-I_F/I_{F0}=f(^qE_P^2)$ (c) of **1** in TOL (a) and $CHCl_3$ (c) for corresponding quenching wavelengths λ_q. Solid black lines are linear fittings (a, c). One-photon STED spectra of **1** (b, curves 3, 4, blue and red circles) in TOL (3, blue circles) and $CHCl_3$ (4, red circles). 2PA spectrum (d, curve 2) and two-photon STED spectrum (d, curve 3) of **1** in $CHCl_3$. Normalized absorption spectra (b, curves 1, 2; d, curve 1) and fluorescence spectra (b, curve 1′, 2′; d, curve 1′) of **1** in TOL (b, curves 1, 1′) and $CHCl_3$ (b, curves 2, 2′; d, curve 1′).

$watermark-text
$watermark-text
$watermark-text

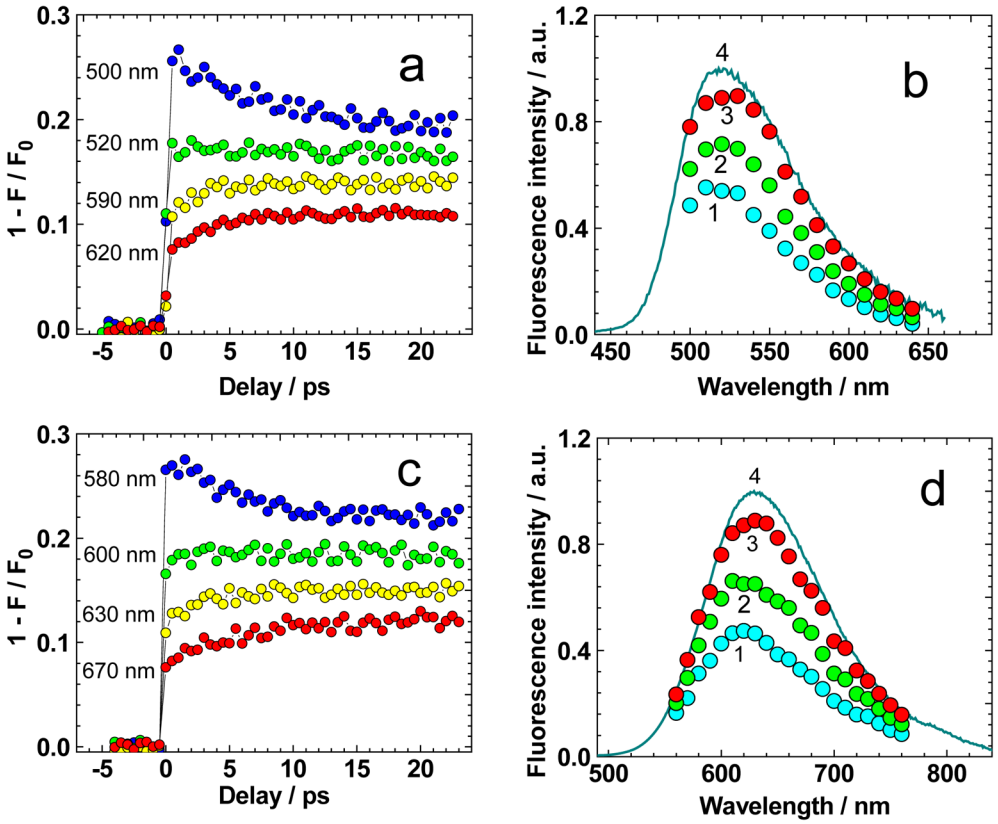

Figure 8.

Transient quenching dependences $1 - I_F/I_{F0} = f(\tau_D)$ (a, c) of **1** in TOL (a) and $CHCl_3$ (c) for corresponding quenching wavelengths λ_q. Time-resolved one-photon STED spectra of **1** (b, d) for $\tau_D = 0$ ps (1, cyan circles), 2 ps (2, green circles), and 6 ps (3, red circles) in TOL (b) and $CHCl_3$ (d). Normalized fluorescence spectra (b, d, curves 4) of **1** in TOL (b) and $CHCl_3$ (d).

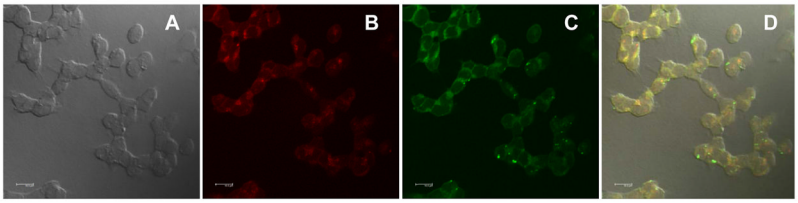

Figure 9.

Confocal fluorescence images of HCT 116 cells incubated with 2PA probe **1** encapsulated in Pluronic® F-127 (20 μM, 1 h) and Lysotracker Red (75 nM, 1 h). DIC (a), one-photon fluorescence image showing Lysotracker Red (b) and 2PA probe **1** encapsulated in Pluronic® F-127 micelles (c). (d) Colocalization (overlay of B and C). 10 μm scale bar.

$watermark-text
$watermark-text
$watermark-text

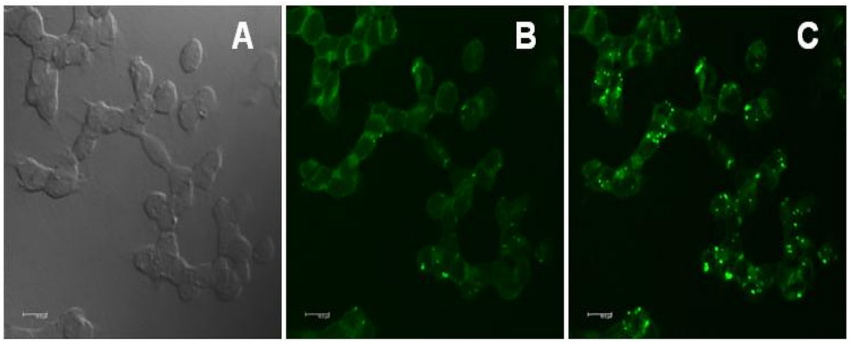

Figure 10.
One-and two-photon fluorescence micrographs of HCT 116 cells incubated with probe **1** encapsulated in Pluronic® F-127 (20 μM, 1 h). DIC (a), one-photon fluorescence (b), and two-photon fluorescence images (c), 80 MHz, 75 fs pulse width tuned to 700 nm, 63x objective. 10 μm scale bar.

$watermark-text
$watermark-text
$watermark-text

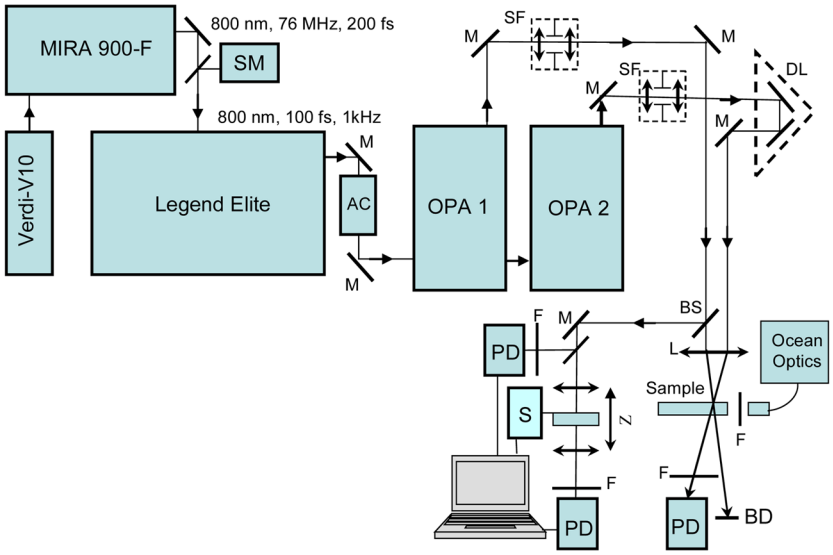

Figure 11.

Simplified schematic diagram of the experimental setup: SM - spectrometer; AC - optical autocorrelator; M - 100% reflection mirrors; BS - beam splitter; SF - space filters; DL - optical delay line with retro-reflector; PD -calibrated Si and/or InGaAs photodetectors; L - focusing lenses; F - set of neutral and/or interferometric filters; S -step motor; Sample – 1-mm flow quartz cuvette with investigated solutions; Z - Z-scan setup; BD - beam dump. Additional details are presented in the text.

$watermark-text
$watermark-text
$watermark-text

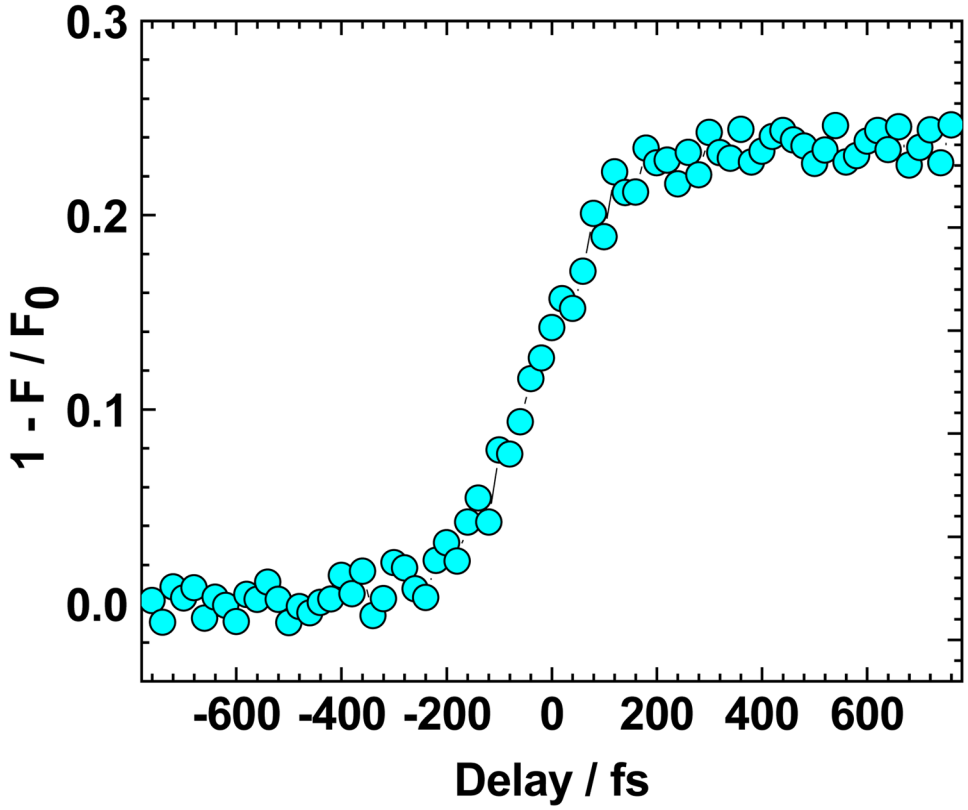

Figure 12.
Typical dependence $1 - I_F/I_{F0} = f(\tau_D)$ for **1** in TOL ($\lambda_q \approx 520$ nm).

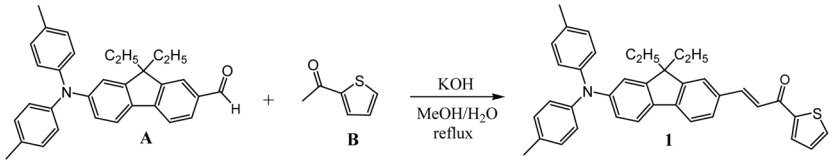

Scheme 1.
Synthesis of chromophore **1**.

$watermark-text
$watermark-text
$watermark-text

$watermark-text $watermark-text $watermark-text

Table 1

Main linear photophysical parameters of **1** in solvents with different polarity Δf and viscosity η: absorption, λ_{ab}^{max} and fluorescence, λ_{fl}^{max}, maxima, Stokes shifts, maxima extinction coefficients, εmax, fluorescence quantum yields, Φ, experimental, τ, and calculated, τ_{cal}, fluorescence lifetimes and photochemical decomposition quantum yields, Φ_{ph}.

N/N	HEX	TOL	$CHCl_3$	THF	ACN
Δf [a]	$3 \cdot 10^{-4}$	0.0135	0.148	0.209	0.305
η, cP	0.31	0.59	0.54	0.48	0.34
λ_{ab}^{max}, nm	420 ±1	433 ±1	445 ±1	430 ±1	427 ±1
λ_{fl}^{max}, nm	462 ±1	520 ±1	629 ±1	593 ±1	540 ±2
Stokes shift, cm^{-1} (nm)	2160 ±100 (42 ±2)	3860 ±100 (87 ±2)	6570 ±100 (184 ±2)	6390 ±100 (163 ±2)	4900 ±100 (113 ±6)
$\varepsilon^{max} * 10^{-3}$, $M^{-1}cm^{-1}$	47 ±3	30 ±2	27 ±2	37 ±2	36 ±2
Φ	0.64 ±0.05	1.0 ±0.05	0.9 ±0.05	1.0 ±0.05	0.01 ±0.003
τ, ns [b]	1.15 ±0.08	2.3 ±0.08	3.5 ±0.08	3.8 ±0.08	-
τ_{cal}, ns	1.82 ±0.2	3.37 ±0.3	3.88 ±0.3	4.0 ±0.3	0.03 ±0.01
$\Phi_{ph} * 10^5$	60 ±1	3 ±0.5	2.6 ±0.5	1.3 ±0.2	3.7 ±0.5

[a] Orientation polarizability $\Delta f = (\varepsilon - 1)/(2\varepsilon + 1) - (n^2 - 1)/(2n^2 + 1)$ (ε and n are the dielectric constant and refraction index of the medium, respectively).

[b] All experimental values of lifetimes were obtained with a goodness-of-fit parameters $\chi^2 \geq 0.99$.

Chemphyschem. Author manuscript; available in PMC 2013 October 22.

$watermark-text

$watermark-text

$watermark-text

Table 2

Calculated energies of the electronic transitions, E_{ij}, oscillator strengths, f_{OS}, and transition dipoles, $\boldsymbol{\mu}_{ij}$, ($i = 0$, 1; $j = 2, 3, \ldots$) of **1**, (TDDFT/6–31(d,p)/B3LYP).

Transition	E_{ij}, eV	f_{OS}	μ_{ij}, D	Main configuration
$S_0 \rightarrow S_1$	2.57	0.631	10.02	0.99 |HOMO→LUMO>
$S_0 \rightarrow S_2$	3.21	0.000	0.0001	0.98 |HOMO3−→LUMO>
$S_0 \rightarrow S_3$	3.58	0.735	7.34	0.90 |HOMO→LUMO+1> −0.38 |HOMO− 1→LUMO>
$S_0 \rightarrow S_4$	3.69	0.269	4.37	0.40 |HOMO→LUMO+1> +0.88 |HOMO−1→LUMO>
$S_0 \rightarrow S_5$	3.87	0.015	1.01	0.95 |HOMO→LUMO+1>
$S_1 \rightarrow S_2$	0.64	0.043	4.22	0.98 |HOMO3−→HOMO>
$S_1 \rightarrow S_3$	1.01	0.003	0.29	0.90 |LUMO→LUMO+1> −0.38 |HOMO−1→HOMO>
$S_1 \rightarrow S_4$	1.12	0.623	12.08	0.40 |LUMO→LUMO+1> +0.88 |HOMO−1→HOMO>
$S_1 \rightarrow S_5$	1.30	0.018	1.91	0.95 |LUMO→LUMO+1>

$watermark-text

$watermark-text

$watermark-text

Table 3

Maximum values of calculated, δ_{2PA}^{cal}, and experimental, δ_{2PA}, 2PA cross sections of **1**.

Two-photon transition	δ_{2PA}^{cal}, GM	δ_{2PA}, GM
$S_0 \rightarrow S_1$	120	400 – 600
$S_0 \rightarrow S_2$	90	50–100
$S_0 \rightarrow S_4$	300	200–350